Title: Inactivity and Ca^{2+} signaling regulate synaptic compensation in motoneurons following hibernation in American bullfrogs

Authors: Tanya Zubov, Lara do Amaral-Silva, Joseph M. Santin*

*Email for correspondence: jmsantin@uncg.edu

Affiliations: [1]The University of North Carolina at Greensboro, Department of Biology

Keywords: homeostatic plasticity, synaptic scaling, AMPA receptor, compensation, control of breathing

Abstract

Neural networks tune synaptic and cellular properties to produce stable activity. One form of homeostatic regulation involves scaling the strength of synapses up or down in a global and multiplicative manner to oppose activity disturbances. In American bullfrogs, excitatory synapses scale up to regulate breathing motor function after inactivity in hibernation, connecting homeostatic compensation to motor behavior. In traditional models of homeostatic synaptic plasticity, inactivity is thought to increase synaptic strength *via* mechanisms that involve reduced Ca^{2+} influx through voltage-gated channels. Therefore, we tested whether pharmacological inactivity and inhibition of voltage-gated Ca^{2+} channels are sufficient to drive synaptic compensation in this system. For this, we chronically exposed *in vitro* brainstem preparations containing the intact respiratory network to tetrodotoxin (TTX) to stop activity and nimodipine to block L-type Ca^{2+} channels. We show that hibernation and TTX similarly increased motoneuron synaptic strength and that hibernation occluded the response to TTX. In contrast, block of L-type Ca^{2+} channels did not alter mean synaptic strength but disrupted the multiplicative scaling of synaptic compensation typically observed in response to hibernation. Thus, inactivity associated with hibernation drives up synaptic strength through mechanisms that do not rely on reduced L-type channel function, while Ca^{2+} signaling independently regulates the balance of synaptic weights. Altogether, these results point to multiple feedback signals for shaping synaptic compensation that gives rise to proper network function during environmental challenges *in vivo*.

Introduction

Neural circuits must produce correct output patterns to generate reliable behaviors. However, animals face constantly changing internal and external environments, posing a threat to stable neuronal function [1]. To maintain stability, the nervous system is thought to use a wide range of homeostatic mechanisms that sense activity perturbations which then modify cellular and synaptic function to regulate neuronal output. Although diverse homeostatic mechanisms exist [2,3], the most well-studied involves compensatory changes in excitatory synaptic strength through a mechanism termed synaptic scaling. Synaptic scaling is interpreted to involve the up or downregulation of all a neuron's synaptic inputs by the same relative amount to oppose activity disturbances [4]. Mounting evidence implicates synaptic scaling in association with diverse physiological conditions such as development [5,6], sleep [7], and learning [8] in mammals, while inappropriate function of homeostatic mechanisms may lead to various neurological disorders [9-11]. Although a large body of work supports cell-wide multiplicative synaptic compensation [4,5,8,12-15], how these processes are regulated and integrated *in vivo* to generate adaptive behaviors is less clear.

Animals that hibernate must enter and exit states of long-term dormancy, making excellent models to connect activity-dependent neural compensation to behavior [16]. Motor circuits that produce breathing in American bullfrogs, *Lithobates catesbeianus*, are especially intriguing in this regard. The respiratory network typically generates stable rhythmic motor activity throughout life. However, during under water hibernation, gas exchange demands are met through cutaneous respiration, and the motor circuits that produce lung breathing stop entirely [17-19]. After months of inactivity, frogs emerge in

the spring and quickly display normal respiratory motor performance [17,20]. We previously found that motoneurons scale up excitatory synapses in response to hibernation, which acts to maintain respiratory motor outflow immediately after the animal restarts breathing [15]. Therefore, this system allows the study of synaptic compensation in relation to motor behavior and points to conserved mechanisms across mammals and amphibians in the natural environment.

In mammalian systems, synaptic compensation is thought to be induced by variables related to inactivity, for example, decreases in firing rate or postsynaptic receptor activation [21-23]. From there, decreases in intracellular calcium represents a message that is proportional to activity, with the capacity to influence Ca^{2+}-dependent signaling that drives compensation [24]. Reduced Ca^{2+} influx through L-type calcium channels in particular plays a critical role in eliciting synaptic compensation in diverse neuronal types [22,25,26]. Given that hibernation causes a large and chronic reduction in neuronal output, inactivity and subsequent reductions in Ca^{2+} influx may trigger synaptic compensation that serves to regulate motor performance [15,16]. However, aquatic hibernation involves diverse physiological changes to the animal [27], raising questions about whether inactivity or other aspects of the organismal environment, such as temperature, feedback to control synaptic compensation. To begin to approach this question, we tested the hypothesis that inactivity and reduced voltage-gated Ca^{2+} channel function are sufficient to drive up synaptic strength in frog respiratory motoneurons. The amphibian respiratory network is well-suited to address this question, as “fictive breathing” motor patterns persist in dissected brainstem preparations for >24 hours *in vitro* [28]. This allowed us to perform chronic pharmacological manipulations to

the native network without the need for cell culture conditions. To this end, we isolated the respiratory network *in vitro*, silenced activity with tetrodotoxin (TTX) or blocked L-type Ca^{2+} channels with nimodipine. We then compared synaptic responses to these manipulations with that seen during hibernation and then tested whether hibernation occludes the synaptic response induced by these drugs. This allowed us to infer whether network inactivity and Ca^{2+} channel blockade overlap with pathways associated with hibernation, a similar “sufficiency/occlusion” approach used to relate long-term potentiation of synaptic strength to learning at hippocampal synapses [29].

Results

Amphibians inflate the lungs with positive pressure, whereby muscles of the buccal floor and glottis form a pump-valve system for lung ventilation. Laryngeal motoneurons that innervate the glottal dilator, the value muscle, (Fig. 1A) undergo compensatory upregulation of AMPA-glutamate receptor currents in response to ~2 months of aquatic hibernation [15]. To simulate the overwintering environment in this study, frogs were cooled from 20°C to 2°C over one week and then held at 2°C for either two or four weeks before assessing synaptic strength in brain slices. Consistent with our previous report with inactivity at longer time scales, synaptic strength, as assessed by the amplitude of spontaneous excitatory postsynaptic currents (sEPSC), increased in frogs exposed to the simulated hibernation environment at both two and four weeks (Fig. 1B) with no change in sEPSC frequency (Fig. 1C). These results confirm postsynaptic compensation in response to hibernation and demonstrate that upregulation of excitatory synaptic strength plateaus at a new steady-state value relatively early into aquatic submergence.

Variables associated with inactivity (*i.e.*, loss of postsynaptic firing or synaptic transmission) can drive homeostatic increases in synaptic strength [21,22]. Our rationale was that if synaptic compensation during winter is responding to inactivity, pharmacological inactivity may produce a similar degree of synaptic compensation as hibernation, thus demonstrating inactivity as a sufficient signal to generate the hibernation response. To test this, we silenced intact respiratory networks in the brainstem-spinal cord preparation with 100 nM TTX for 16 hours (Fig. 2A). While the time course of hibernation (one month) and shorter-term TTX (16 hours) are different,

synaptic scaling has been observed to manifest after 4 hours of inactivity *in vitro* [22]. We compared average miniature excitatory postsynaptic current amplitude in slices (mESPCs) following network activity induced by TTX to Time Controls (control preparations with rhythmic activity present for 16 hrs at 22°C) and Post-Hibernation preparations (preparations recovered following hibernation for 16 hrs at 22°C; Fig 2A). TTX and hibernation groups exhibited similar mean increases in cell-averaged mEPSC amplitude relative to Time Control preparations. These mean increases were not different from each other (Fig. 2B-C). Therefore, pharmacological inactivity produces a similar average amount of synaptic compensation as physiological inactivity in hibernation.

The previous experiment demonstrated that inactivity *via* TTX is sufficient to drive synaptic compensation in this system. Next, we determined if hibernation occludes the synaptic response to TTX. If hibernation prevents further increases by TTX, this may reflect overlapping signaling processes. However, if TTX and hibernation produce additive responses, this may suggest divergent signaling pathways for compensation. When we exposed post-hibernation preparations to TTX for 16 hr, we did not observe further increases in synaptic strength by TTX compared to hibernation alone (Fig. 3A-B). Membrane properties, mEPSC frequency, and mEPSC decay time constant were not different across control, post-hibernation, TTX, and post-hibernation+TTX groups (Fig. 4). Therefore, these data suggest that hibernation occludes the synaptic compensation response to TTX.

To upregulate synaptic strength in an inactivity-dependent manner, we hypothesized that reduced Ca^{2+} influx through voltage-gated Ca^{2+} channels may play a

role. Thus, we exposed rhythmic circuit preparations to 10 µM nimodipine, a blocker of L-type Ca^{2+} channels in motoneurons of this system [30]. Exposure of warm-acclimated preparations to nimodipine did not affect mean mEPSC amplitude or the distribution relative to warm-acclimated time controls (Fig. 5A-B). Therefore, block of L-type Ca^{2+} does not mimic the synaptic response to TTX and hibernation. Post-hibernation preparations exposed to nimodipine still resulted in upregulation of cell-averaged mEPSCs compared to time controls (Fig 5A-B), just as we observed with TTX, hibernation, and hibernation+TTX. When comparing the post-hibernation+nimodipine group to post-hibernation alone, mEPSC amplitude were not different ($p=0.470$, Fig. 3C). Overall, reduced L-type channel function does not drive compensation in this system.

Given that the entire mEPSC amplitude distribution is thought to be regulated by a multiplicative scaling factor during inactivity [24], we tested whether the increase in postsynaptic strength in each of our experimental conditions increases according to a multiplicative scaling rule. We used the rank-order method to test for synaptic scaling of mESPC amplitudes in populations of neurons [4,8,31]. To do this, mEPSCs from control and treatment groups (TTX, hibernation, hibernation+TTX, hibernation+nimodipine) were rank-ordered from the smallest to largest amplitude, plotted against each other (ranked control vs. ranked treatment), and fit with a linear regression. The treatment distribution for each form of inactivity was then mathematically downscaled by the equation of the line, and the scaled distribution was compared to control. Positive evidence for multiplicative scaling is usually taken as a statistically indistinguishable matching between the scaled and control distributions of mEPSC amplitudes [12,32].

As expected, all treatments strongly right-shifted the amplitude distribution of mEPSCs relative to controls, as expected based on the mean upregulated synaptic strength for all conditions (Fig. 6A-E; K-S test; time control vs. all treatment conditions; $p<0.0001$). When we performed the downscaling transformation on each treatment distribution, interestingly, not all showed evidence of multiplicative synaptic scaling. Hibernation and hibernation+TTX, led to multiplicative scaling (Fig. 6B-C), but TTX alone (Fig. 6A) and hibernation in the presence of nimodipine (Fig. 6D-E) did not. These results indicate that hibernation upregulates synaptic drive while maintaining the balance of synaptic weights according to scaling rule as we previously showed [15]. However, the scaling organization appears to be regulated or maintained by active Ca^{2+} signaling through L-type channels, as blocking voltage-gated Ca^{2+} channels disorganized the scaling relationship typical of hibernation.

To infer the role of these synaptic modifications on network function, we assessed circuit activity of the intact respiratory network. The respiratory network is a central pattern generating network which permits the recording of these motor neurons as a receive their normal presynaptic inputs *ex vivo* (Fig. 7A). In this preparation, extracellular population motor burst frequency of the cut nerve root provides information regarding the function of the rhythm generating networks [33], and integrated burst shape relates to motoneuron firing and/or recruitment [34]. Thus, we were able to observe physiological motor output from motoneurons under conditions with no changes in synaptic strength (control and warm-nimodipine), upregulated and scaled synaptic strength (post-hibernation), and upregulated but not scaled synaptic strength (post-hibernation+nimodipine). Across controls, post-hibernation, and post-

hibernation+nimodipine, no differences existed in frequency of the respiratory rhythm at 13 hrs *in vitro* (one-way ANOVA, p=0.3215). However, preparations treated with nimodipine after hibernation had shorter motor burst widths relative to all other groups after 13 hrs (Fig. 7 B-C). Burst width narrowing appeared to be a chronic effect induced by nimodipine following hibernation, as acute application did not affect burst width before and after winter, and all preparations without nimodipine (control or post-hibernation) did not change with time (Fig. 7C). In addition, membrane potential, input resistance, and action potential firing frequency were not different across groups, indicating chronic nimodipine does not induce changes in intrinsic membrane properties (Fig. 7D-F). Overall, these experiments suggest that inactivity scales up synaptic strength in response to hibernation and proper scaling of the mESPC distribution appears to be important for normal network function associated with breathing after hibernation.

Discussion

Neural circuits can compensate for activity perturbations with the apparent goal of regulating neuronal output. American bullfrogs must produce appropriate motor drive for breathing after potentially months of network inactivity during hibernation. Our previous results showed that scaling up the strength of motoneuron synapses helps promote motor output after hibernation to generate breathing. Data here support the idea that inactivity during hibernation plays a key role in this response. However, upregulation of synaptic strength did not occur *via* the reduction of Ca^{2+}-dependent signaling through L-type Ca^{2+} channels as occurs in other models of synaptic compensation. On the other hand, the precise distribution of synaptic weights is maintained by Ca^{2+}-sensitive feedback after hibernation to support motor performance. Overall, these results suggest that multiple signals interact to regulate synaptic compensation in response to environmental challenges *in vivo*.

Inactivity drives up synaptic strength in response to hibernation

Decades of work support the view that neurons upregulate synaptic strength in response to inactivity. Given that cold temperatures silence the respiratory network [17,18], we hypothesized that inactivity may trigger scaling up of synaptic strength in response to hibernation. Previously, we showed that synaptic strength is increased at ~2 months of hibernation. Here we demonstrate that increases in synaptic drive are present at 2 weeks into aquatic hibernation, which then saturate a new steady-state level (Fig. 1B). These responses were comparable to inactivity by TTX (Fig. 2C) and are therefore consistent with upregulation of synaptic strength in response to a signal related to inactivity. Further supporting this conclusion, TTX did not cause greater increases in

synaptic strength when applied after hibernation, which suggests the mechanisms involved in enhancing synaptic strength were already engaged by hibernation. In this regard, inactivity may upregulate synaptic strength through mechanisms that involve the loss of spiking, reduced AMPA receptor activation, and reduced neuromodulation [21,35,36]. That said, synaptic compensation does not seem to strictly follow negative feedback regulation as predicted for activity-dependent homeostatic plasticity. First, inactivity over vastly different time scales (16 hours to 1 month) produced similar degrees of mean synaptic strengthening. This is inconsistent with compensation that follows the accumulation of an error signal over time while the neuron remains below its set point [4,37]. Additionally, synaptic strength remained elevated despite the return of activity for at least 16 hrs after hibernation and did not differ when activity was present or absent during the post-hibernation period. Thus, our results indicate that inactivity likely drives up synaptic strength but a more complicated regulation scheme appears to influence the maintenance of this plasticity.

The previous results indicated that inactivity plays a role in driving up synaptic strength. L-type Ca^{2+} channels are attractive effectors of this response as they communicate changes in intracellular Ca^{2+} to the nucleus and other intracellular signaling pathways that elicit synaptic compensation during inactivity [22,25]. Thus, we inhibited L-type Ca^{2+} channels to understand if the “inactivity signal” during hibernation and TTX involved reduced L-type Ca^{2+} channel activity. In contrast to this hypothesis, chronic block of L-type Ca^{2+} channels did not affect mEPSC amplitude. Although our data rule out the possibly for a role by nimodipine-sensitive L-type Ca^{2+} channels in compensation, other Ca^{2+} channels may contribute. For example, in respiratory motor

neurons of this species, nimodipine blocks the high-voltage activated Ca^{2+} current by ~30-40% [30], indicating the expression of other somatodendritic calcium channels on respiratory motoneurons. Nevertheless, L-type Ca^{2+} channels do not appear to drive synaptic compensation, differing from traditional models in neuronal cultures [22,25,26,38]. Future work should address the signaling processes that read out inactivity to initiate and maintain synaptic compensation throughout hibernation.

L-type Ca^{2+} channels maintain multiplicative scaling after hibernation

As a compensation response, synaptic inputs are often upregulated across the entire distribution by the same multiplicative factor [4]. An interesting finding of this study is hibernation, but not TTX, led to multiplicative scaling when we performed the standard rank-order test [4,8,14]. In line with our results, TTX applied to the hippocampus *in vivo* drives up synaptic strength without evidence of scaling as determined by the rank-order test [39]. Additionally, a recent study also suggested that TTX may not lead to uniform scaling in different mammalian neuronal types when assessed using the rank-order method [40], although there is significant evidence to the contrary [12,22,41,42]. While we used the standard method to infer the presence or absence of scaling, we note recent studies suggesting complexity in this interpretation. Specifically, synaptic spine density and AMPAR expression across individual synapses do not scale uniformly within the same neuron even though multiplicative scaling appears to occur at the population level [43,44]. A non-zero y-intercept in the linear model used to test for scaling may also suggest that additive processes work alongside multiplicative mechanisms [41]; however, the y-intercept has been interpreted to account for mEPSCs that fall below the

detection cutoff to align control and scaled distributions for the assessment of multiplicative scaling [4,32]. In support of the later possibility, the y-intercept values we obtained in the two hibernation groups that exhibited evidence for multiplicative scaling compensated for our 7pA cutoff within <0.1pA. Therefore, our data support the idea that excitatory synapses scale up in response to hibernation, but the multiplicative organization appears to be controlled by mechanisms associated with the winter state rather than inactivity *per se*.

What signals coordinate the multiplicative scaling in response to hibernation? An interesting finding of this study was that blocking L-type Ca^{2+} channels *following* hibernation disrupted multiplicative scaling across the mEPSC distribution without influencing the average synaptic compensation. These results indicate that Ca^{2+} feedback is a signal for maintenance of the scaled synaptic amplitude distribution after hibernation. Given that we observed evidence for multiplicative scaling after hibernation in the presence of TTX, the sum of our data suggests that the maintenance of synaptic compensation in the “scaled state” is, therefore, Ca^{2+}-dependent but not activity-dependent. As intracellular calcium transients tend to follow patterned activity, these results may appear contradictory. However, spontaneous neurotransmitter release in silent neurons can activate L-type channels at subthreshold voltages to induce neuronal plasticity [45,46], suggesting a spike-independent role for Ca^{2+} to maintain the scaling organization. Results in the present study pertain to the maintenance of scaling soon after hibernation; yet, as cold temperature increases membrane input resistance [47,48], spontaneous neurotransmitter release may cause larger postsynaptic depolarizations compared to warm animals, generating significant Ca^{2+} influx through L-type channels to

orchestrate scaling even during the winter. Altogether, our results seem to diverge from classic models of synaptic scaling, whereby a multiplicative scaling factor drives up synaptic strength during inactivity. Instead, our data suggest that inactivity upregulates synaptic strength through mechanisms that do not involve multiplicative scaling (Fig. 6A), and a separate regulatory system involving L-type Ca^{2+} channels is engaged by the "winter state" to organize the balance of the mEPSC distribution (Fig. 6D-E). Given that we can effectively disrupt the scaling with nimodipine, but leave overall compensation intact following hibernation, provides evidence to this assertion. The mechanisms that control these parallel signaling pathways for compensation and the scaling organization warrant further investigation and may be relevant to complex physiological perturbations in other systems.

Synaptic compensation and regulation of respiratory motor output

Our previous study identified that upregulation of synaptic strength acts to maintain motor output associated with breathing following hibernation [15]. In this study we had the unique opportunity to study this network in states where motoneurons had compensated with (hibernation) and without (hibernation+nimodipine) scaled synapses. Results here argue for the role of precise multiplicative scaling in the regulation of motor function. We draw this conclusion because population motor output for breathing was reduced when synaptic strength of motoneurons was upregulated but not correctly scaled after hibernation (Fig. 7). We recognize the challenge of attributing changes in network-level properties to subtle shifts in the distribution of synaptic weights on motoneurons, and we made several attempts to address other variables that could explain these results. First, rhythmic burst frequency of the network was the same

across all groups *ex vivo*; thus, overall activity differences and altered rhythm generator function is unlikely to explain shorter motor bursts. Second, several intrinsic membrane properties were not different across scaled and “unscaled” conditions (Fig. 7D-F), suggesting that changes in excitability did not weaken the motor outflow. Third, exposing warm-acclimated control preparations to nimodipine before hibernation did not affect the amplitude distribution of mEPSCs, motor burst width, or any other obvious electrophysiological property, arguing against other actions of nimodipine on different parts of the network (Fig. 6-7). Finally, acute exposure to nimodipine did not affect burst duration in any group (Fig. 7C), suggesting that slow disruption of Ca^{2+} feedback after hibernation alters synaptic organization that shapes burst duration rather than acute effects of calcium channel blockade on network excitability. All of this said, we cannot state with certainty if narrower respiratory bursts after hibernation in the presence of nimodipine reflect improperly scaled synapses on motoneurons (Fig. 6D-E) or other actions of nimodipine on premotor neurons that regulate motor outflow in a hibernation-dependent manner. Nevertheless, these results, in concert with our previous findings [15], suggest that synaptic scaling is important for regulating motor performance shortly after inactivity in hibernation. Future work must aim to understand how a failure to accurately scale motoneurons synapses translates to altered respiratory-driven firing responses at the single neuron level.

Conclusion

Compensation *via* postsynaptic AMPA receptor currents is a well-documented response to reduced activity across diverse neurons and systems. Proper synaptic compensation has clear adaptive value following hibernation in the frog, as it ensures

adequate motor drive for lung ventilation (15; present study Fig. 5). More broadly, our results suggest that homeostatic synaptic plasticity could represent a more complicated regulation scheme when studied in the context of living animals in response to natural perturbations. Synaptic compensation is often viewed as a conceptually simple feedback process, whereby neurons sense their activity state and elicit appropriate compensation in attempt to regulate firing or network output. In contrast, our data suggest that different aspects of the same compensation response, for example the mean synaptic drive and the scaled nature of the synaptic amplitude distribution, may be controlled by different variables. Along these lines, many neurological disorders are thought to involve a failure of homeostatic synaptic and intrinsic mechanisms [9], all of which occur in complex organisms with diverse types of environmental feedback onto the nervous system. Our data suggest confronting how the environment shapes compensation is necessary to understand the expression and control of homeostatic compensation. Learning from animals that use these mechanisms to survive in their natural environments, therefore, has the potential to provide new insight into how neuronal function in regulated in both health and disease states.

Materials and Methods

Animals

Bullfrogs of either sex weighing approximately 100 g were purchased from Rana Ranch (Twin Falls, ID, USA). Control frogs were maintained at 20 ºC in plastic tubs and were provided aerated water with access to wet and dry areas. Frogs were fed pellets provided by Rana Ranch once per week. Hibernation conditions were simulated in temperature controlled incubators. The temperature of water was lowered from 20ºC to 2ºC over the course of a week, dropping about 2-3 degrees per day. On the seventh day, a plastic screen was placed at the top of the water to block to prevent access to the surface. Animals do not eat at cold temperatures; therefore, food was also withheld while frogs remained at 2°C. All frogs in each condition were kept on a 12 hr:12 hr light: dark cycle. Experiments were only performed during the light cycle.

Dissection and Tissue Preparation

Brainstem-spinal cord dissections were performed as previously described [15]. Briefly, frogs were deeply anesthetized with approximately 1 ml of isoflurane per liter and rapidly decapitated. The head was immersed in chilled bullfrog artificial cerebrospinal fluid (aCSF) and the brainstem-spinal cord was removed, keeping the motor rootlets of the vagus intact (aCSF; concentrations in [mM]: 104 NaCl, 4 KCl, 1.4 $MgCl_2$, 7.5 glucose, 40 $NaHCO_3$, 2.5 $CaCl_2$ and 1 NaH_2PO_4, and gased with 98.5% O_2, 1.3%CO_2; pH = 7.85). Following the dissection, the brain was superfused with aCSF with a flow rate of ~6 mL per minute.

To selectively label laryngeal branch motoneurons that innervate the glottal dilator, the 4th branch of the vagus nerve was isolated and then backfilled tetramethylrhodamine dextran 3000 MW (Life Technologies Corporation, Eugene, OR USA). Approximately 1 uL of 10% dextran was loaded into the tip of a glass pipette that fit snuggly around the cut 4th root of the vagus, as this nerve contains axons that mainly innervate the glottal dilator see references provided in [15]. Backfills lasted two hours and produced robustly labeled neurons for electrophysiological recording. Following the dye loading process, tissue was sliced with a vibratome at 300 µM. Sections approximately 300-600 µm rostral to the obex were used for electrophysiological recording. Tissue slices were left to recover for an hour before electrophysiological recording.

Whole-cell patch clamp recordings

Slices containing labeled motoneurons were transferred to the recording chamber, stabilized with a nylon grid, and exposed to aCSF at a flow rate of ~1-2 mL per min supplied via a gravity-fed system. The region containing labeled neurons was imaged at 4x, and then individual neurons were located within the slice at 60x (excitation, 540 nm: emission, 605 nm). Imaging was performed with a Hamamatsu ORCA Flash 4.0LT sCMOS Camera (Hamamatsu Photonics, Japan). Identified neurons were approached with the whole-cell patch pipette controlled by a Sutter Instruments micromanipulator system, which was equipped with a MP-285 micromanipulator and a MPC-200 controller (Sutter Instruments, CA, USA). A P87 horizontal pipette puller (Sutter Instruments, Novato, CA, USA) was used to pull patch pipette, which had resistances of 2-3 MΩ when filled with solution containing the follow composition (in mM): 110 K-gluconate, 2 $MgCl_2$, 10 HEPES, 1 Na_2-ATP, 0.1 Na_2-GTP, 2.5 EGTA. The

cell of interest was approached with gentle positive pressure on the pipette. When an indentation could be seen on the cell in the bright field with IR-DIC optics, positive pressure was removed and a >1 GΩ was formed by applying slight negative pressure through the pipette by mouth. Whole-cell access was obtained by rapid negative pressure applied by mouth to rupture the GΩ seal. For measurements of excitatory postsynaptic currents, cells were voltage clamped at -80 mV to record synaptic currents mediated by AMPA receptors [15]. When spontaneous excitatory synaptic currents (sEPSCs) were recorded in aCSF, no TTX was included during the recording. When miniature excitatory postsynaptic currents (mESPCs) were recorded, 500 nM TTX was added the aCSF. A +10 mV step was periodically performed to estimate series resistance (peak of the transient current) and input resistance (steady-state current) using Ohm's law. Measurements of membrane potential were made in current clamp, and firing rate was assessed at 3X rheobase in some current clamp prior to the application of TTX to measure mEPSCs. We often recorded more than one neuron per slice; however, TTX does not have a fast washout time in this preparation; therefore, firing properties in current clamp were not assessed for every cell. Previous work in these neurons suggests that firing response to current injection does not change in these neurons following hibernation [15], and our results in this study, despite a smaller sample size, support this previous finding.

Experimental Treatments

Three main series of experiments were performed in this study: (1) those that varied the duration of cold acclimation and then assessed synaptic function immediately after removing the animal from the hibernation environment (Supplemental Fig. 1), (2) those

that used either warm-acclimated control animals or 1 month hibernation animals and then exposed these brainstem preparations to TTX for 16 hrs in vitro (Fig 1-2 Supplemental Fig. 2-4), and (3) those that used either warm-acclimated control animals or 1 month hibernation animals and exposed each to 10 µM nimodipine for 16 hrs (Fig 3-4). For series 1 experiments control frogs (20°C) or cold-acclimated (2°C for 2 or 4 weeks) were used, and then synaptic function was assessed after animals were removed from these environments to roughly determine the time course of synaptic compensation. In series two experiments our main goal was to compare to post-hibernation synaptic function to inactivity with 100 nM TTX. In addition, we assessed synaptic function in post-hibernation animals after silencing rhythmic motor output with TTX. TTX silenced all preparations for the entire 16 hr period (data not shown). In series three experiments, we exposed warm-acclimated control and post-hibernation rhythmic preparations to 10 µM nimodipine for 16 hrs to block L-type Ca^{2+} channels in frog respiratory motoneurons [30], and a separate time control group was run in parallel. Following these treatments all synaptic recordings were performed in standard aCSF with 500 nM TTX. Extracellular output from the cut vagus nerve via a bipolar suction electrode connected to an A-M Systems Model 1700 amplifier (bandpass filtered between 10-1000 Hz, 100X gain). Activity of this nerve is primarily generated by the 4th branch of the vagus nerve (the same neurons we studied in slices), and provides the main drive to the glottal dilator, which gates airflow into and out of the lung in anuran amphibians [49].

Data Analysis

All data analysis was performed using the peak analysis module on LabChart 8 (ADInstruments, Sydney, Australia). sEPSC and mESPCs events were recorded for 30 seconds and averaged to estimate excitatory synaptic drive due to AMPAR transmission. Cutoff amplitude was set at 7 pA. All analyses were checked by eye to verify EPSCs were correctly identified. To infer synaptic scaling, we used the standard rank-order method as originally described by Turrigiano et al. [4]. Briefly, a series of 50 mESPCs were chosen for each cell in the group and the entire distribution was ranked from lowest to highest for control and treatment conditions. In some cases, control and treatment conditions had different numbers of cells. In these situations, cells were randomly removed for the scaling analysis by assigning a number to each cell and then using a random number generator chose which cell(s) would be removed. This allowed equal number of mESPCs to be ranked and scaled in each group. Ranked data were plotted and then fit by a linear regression to obtain the slope of the line and intercept for the entire population. ~5-10 mEPSC events in each group showed extreme values that deviated from the line. These events may be caused by activation of subsaturated AMPA receptors, as suggested previously (23), and were therefore removed for the fitting of the ranked data. Each mESPC event in the treatment distribution was then mathematically downscaled by the equation of the fit from the linear regression and plotted as cumulative distributions. Input and series resistances were calculated by making a 10 mV step, from -80 mV to -70 mV. Series resistance did not vary across groups, and cells with series resistance of >25MΩ were discarded.

Statistics:

Data were analyzed and plotted using GraphPad Prism. Comparisons between two groups were made using a two-tailed unpaired t test. When standard deviations were different between groups, a Welch's test was applied. Analyses involving three or more groups were performed using a one-way ANOVA and followed by Holm-Sidak's multiple comparisons test. When comparing two cumulative distributions, the Kolmogorov Smirnov test was run. When comparing two cumulative distributions, the Kolmogorov Smirnov test was run. Significance was accepted at $p<0.05$.

Acknowledgements: This research was funded in part by the Department of Defense (W911NF2010275), the National Institutes of Health (1R01NS114514 and 1R15NS112920), and lab startup funds from UNC-Greensboro to J.M.S.

Competing Interests: The authors declare no competing interests.

References:

1 Marder, E. & Goaillard, J.-M. Variability, compensation and homeostasis in neuron and network function. *Nature Reviews Neuroscience* **7**, 563-574 (2006).

2 Davis, G. W. Homeostatic signaling and the stabilization of neural function. *Neuron* **80**, 718-728 (2013).

3 Turrigiano, G. Too many cooks? Intrinsic and synaptic homeostatic mechanisms in cortical circuit refinement. *Annual review of neuroscience* **34**, 89-103 (2011).

4 Turrigiano, G. G., Leslie, K. R., Desai, N. S., Rutherford, L. C. & Nelson, S. B. Activity-dependent scaling of quantal amplitude in neocortical neurons. *Nature* **391**, 892-896 (1998).

5 Desai, N. S., Cudmore, R. H., Nelson, S. B. & Turrigiano, G. G. Critical periods for experience-dependent synaptic scaling in visual cortex. *Nature neuroscience* **5**, 783-789 (2002).

6 Pratt, K. G. & Aizenman, C. D. Homeostatic regulation of intrinsic excitability and synaptic transmission in a developing visual circuit. *Journal of Neuroscience* **27**, 8268-8277 (2007).

7 Diering, G. H. *et al.* Homer1a drives homeostatic scaling-down of excitatory synapses during sleep. *Science* **355**, 511-515 (2017).

8 Wu, C.-H., Ramos, R., Katz, D. B. & Turrigiano, G. G. Homeostatic synaptic scaling establishes the specificity of an associative memory. *Current Biology* (2021).

9 Dickman, D. & Wondolowski, J. Emerging links between homeostatic synaptic plasticity and neurological disease. *Frontiers in cellular neuroscience* **7**, 223 (2013).

10 Styr, B. & Slutsky, I. Imbalance between firing homeostasis and synaptic plasticity drives early-phase Alzheimer's disease. *Nature neuroscience*, 1 (2018).

11 Wolfart, J. & Laker, D. Homeostasis or channelopathy? Acquired cell type-specific ion channel changes in temporal lobe epilepsy and their antiepileptic potential. *Frontiers in physiology* **6**, 168 (2015).

12 Gainey, M. A., Hurvitz-Wolff, J. R., Lambo, M. E. & Turrigiano, G. G. Synaptic scaling requires the GluR2 subunit of the AMPA receptor. *Journal of Neuroscience* **29**, 6479-6489 (2009).

13 Gainey, M. A., Tatavarty, V., Nahmani, M., Lin, H. & Turrigiano, G. G. Activity-dependent synaptic GRIP1 accumulation drives synaptic scaling up in response to action potential blockade. *Proceedings of the National Academy of Sciences* **112**, E3590-E3599 (2015).

14 Lambo, M. E. & Turrigiano, G. G. Synaptic and intrinsic homeostatic mechanisms cooperate to increase L2/3 pyramidal neuron excitability during a late phase of critical period plasticity. *Journal of Neuroscience* **33**, 8810-8819 (2013).

15 Santin, J. M., Vallejo, M. & Hartzler, L. K. Synaptic up-scaling preserves motor circuit output after chronic, natural inactivity. *eLife* **6** (2017).

16 Santin, J. M. Motor inactivity in hibernating frogs: Linking plasticity that stabilizes neuronal function to behavior in the natural environment. *Developmental neurobiology* (2019).

17 Santin, J. M. & Hartzler, L. K. Activation of respiratory muscles does not occur during cold-submergence in bullfrogs, Lithobates catesbeianus. *Journal of Experimental Biology* **220**, 1181-1186 (2017).
18 Morales, R. D. & Hedrick, M. S. Temperature and pH/CO_2 modulate respiratory activity in the isolated brainstem of the bullfrog *Rana catesbeiana*. *Comp Biochem Physiol- A Mol Int Physiol* **132**, 477-487 (2002).
19 Vallejo, M., Santin, J. M. & Hartzler, L. K. Noradrenergic modulation determines respiratory network activity during temperature changes in the in vitro brainstem of bullfrogs. *Respiratory physiology & neurobiology* **258**, 25-31 (2018).
20 Santin, J. M. & Hartzler, L. K. Control of lung ventilation following overwintering conditions in bullfrogs, Lithobates catesbeianus. *Journal of Experimental Biology* **In press, doi:10.1242/jeb.136259**, doi:10.1242/jeb.136259 (2016).
21 Fong, M.-f., Newman, J. P., Potter, S. M. & Wenner, P. Upward synaptic scaling is dependent on neurotransmission rather than spiking. *Nature communications* **6** (2015).
22 Ibata, K., Sun, Q. & Turrigiano, G. G. Rapid synaptic scaling induced by changes in postsynaptic firing. *Neuron* **57**, 819-826 (2008).
23 Mahamed, S., Strey, K. A., Mitchell, G. S. & Baker-Herman, T. L. Reduced respiratory neural activity elicits phrenic motor facilitation. *Respiratory physiology & neurobiology* **175**, 303-309 (2011).
24 Turrigiano, G. Homeostatic synaptic plasticity: local and global mechanisms for stabilizing neuronal function. *Cold Spring Harbor perspectives in biology* **4**, a005736 (2012).
25 Wang, H.-L., Zhang, Z., Hintze, M. & Chen, L. Decrease in calcium concentration triggers neuronal retinoic acid synthesis during homeostatic synaptic plasticity. *Journal of Neuroscience* **31**, 17764-17771 (2011).
26 Thiagarajan, T. C., Lindskog, M. & Tsien, R. W. Adaptation to synaptic inactivity in hippocampal neurons. *Neuron* **47**, 725-737 (2005).
27 Tattersall, G. J. & Ultsch, G. R. Physiological ecology of aquatic overwintering in ranid frogs. *Biological Reviews* **83**, 119-140 (2008).
28 McLean, H., Kimura, N., Kogo, N., Perry, S. F. & Remmers, J. E. Fictive respiratory rhythm in the isolated brainstem of frogs. *Journal of Comparative Physiology A* **176**, 703-713 (1995).
29 Whitlock, J. R., Heynen, A. J., Shuler, M. G. & Bear, M. F. Learning induces long-term potentiation in the hippocampus. *science* **313**, 1093-1097 (2006).
30 Bueschke, N., Amaral-Silva, L. d., Hu, M. & Santin, J. M. Lactate ions induce synaptic plasticity to enhance output from the central respiratory network. *The Journal of physiology*.
31 Pacheco, A. T., Bottorff, J., Gao, Y. & Turrigiano, G. G. Sleep promotes downward firing rate homeostasis. *Neuron* **109**, 530-544. e536 (2021).
32 Blackman, M. P., Djukic, B., Nelson, S. B. & Turrigiano, G. G. A critical and cell-autonomous role for MeCP2 in synaptic scaling up. *Journal of Neuroscience* **32**, 13529-13536 (2012).
33 Greer, J., Smith, J. & Feldman, J. Role of excitatory amino acids in the generation and transmission of respiratory drive in neonatal rat. *The Journal of physiology* **437**, 727-749 (1991).

34 Johnson, S. M., Wilkerson, J. E., Wenninger, M. R., Henderson, D. R. & Mitchell, G. S. Role of synaptic inhibition in turtle respiratory rhythm generation. *The Journal of physiology* **544**, 253-265 (2002).
35 Santin, J. M. & Schulz, D. J. Membrane voltage is a direct feedback signal that determines ion channel expression patterns in neurons. *Current Biology* **in press** (2019).
36 Khorkova, O. & Golowasch, J. Neuromodulators, not activity, control coordinated expression of ionic currents. *Journal of Neuroscience* **27**, 8709-8718 (2007).
37 Wierenga, C. J., Ibata, K. & Turrigiano, G. G. Postsynaptic expression of homeostatic plasticity at neocortical synapses. *Journal of Neuroscience* **25**, 2895-2905 (2005).
38 Joseph, A. & Turrigiano, G. G. All for one but not one for all: Excitatory synaptic scaling and intrinsic excitability are coregulated by CaMKIV, while inhibitory synaptic scaling is under independent control. *Journal of Neuroscience*, 0618-0617 (2017).
39 Echegoyen, J., Neu, A., Graber, K. D. & Soltesz, I. Homeostatic plasticity studied using in vivo hippocampal activity-blockade: synaptic scaling, intrinsic plasticity and age-dependence. *PloS one* **2**, e700 (2007).
40 Hanes, A. L. *et al.* Divergent synaptic scaling of miniature epscs following activity blockade in dissociated neuronal cultures. *Journal of Neuroscience* **40**, 4090-4102 (2020).
41 Kim, J., Tsien, R. W. & Alger, B. E. An improved test for detecting multiplicative homeostatic synaptic scaling. *PloS one* **7**, e37364 (2012).
42 Louros, S. R., Hooks, B. M., Litvina, L., Carvalho, A. L. & Chen, C. A role for stargazin in experience-dependent plasticity. *Cell reports* **7**, 1614-1625 (2014).
43 Wang, G., Zhong, J., Guttieres, D. & Man, H.-Y. Non-scaling regulation of AMPA receptors in homeostatic synaptic plasticity. *Neuropharmacology* **158**, 107700 (2019).
44 Barnes, S. J. *et al.* Deprivation-induced homeostatic spine scaling in vivo is localized to dendritic branches that have undergone recent spine loss. *Neuron* **96**, 871-882. e875 (2017).
45 Li, Y., Gorassini, M. A. & Bennett, D. J. Role of persistent sodium and calcium currents in motoneuron firing and spasticity in chronic spinal rats. *Journal of neurophysiology* **91**, 767-783 (2004).
46 Li, B. *et al.* Neuronal Inactivity Co-opts LTP Machinery to Drive Potassium Channel Splicing and Homeostatic Spike Widening. *Cell* (2020).
47 Santin, J. & Hartzler, L. Temperature influences CO_2/pH-sensitivity in locus coeruleus neurons of the bullfrog, *Lithobates catesbeianus*. *FASEB J* **27** (2013).
48 Santin, J. & Hartzler, L. Activation state of the hyperpolarization-activated current (Ih) modulates temperature-sensitivity of firing in locus coeruleus neurons from bullfrogs. *American journal of physiology. Regulatory, integrative and comparative physiology* **308**, R1045-R1061 (2015).
49 Sakakibara, Y. The pattern of respiratory nerve activity in the bullfrog. *The Japanese journal of physiology* **34**, 269-282 (1983).

Figures and Legends

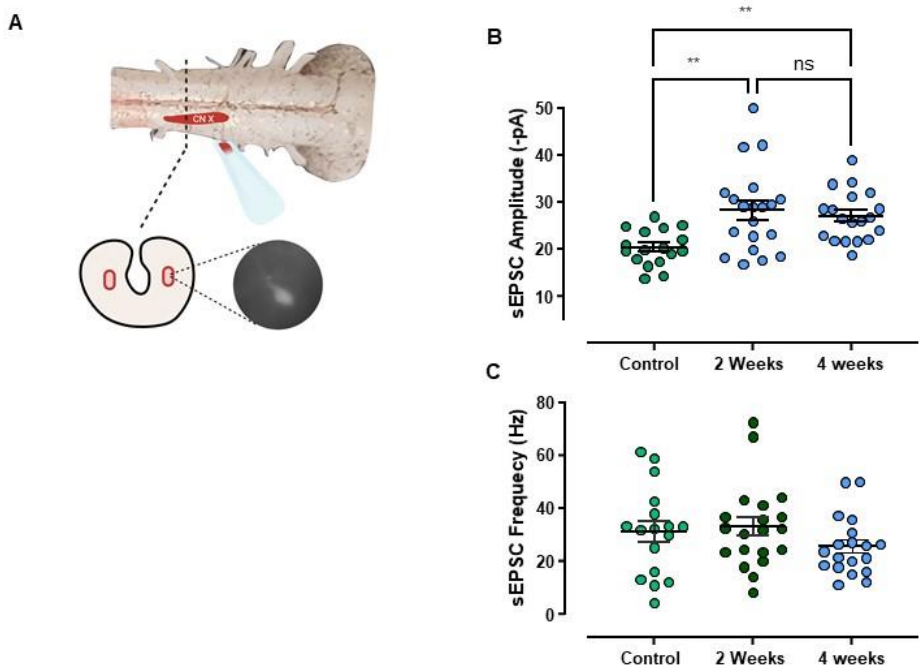

Figure 1 sEPSC amplitude, but not frequency, increases by two weeks of cold-acclimation. (A) Schematic of the experimental process to label respiratory motoneurons. The 4th root of the vagus nerve was backfilled with fluorescent dextran, and neurons were identified in slices through fluorescence imaging microscopy. Animals were either warm-acclimated (control; 22°C; n=17), or cold-acclimated for two (n=20) or four weeks (n=19). (B) sEPSC amplitude (One-way ANOVA; p=0.0013) but not frequency (One-way ANOVA; (C) was increased by 2 weeks and remained elevated at four weeks. Circles represent cell-averaged mEPSCs for each neuron. Error bars are S.E.M. Horizontal line represents the mean. **p<0.01. Error bars are S.EM.

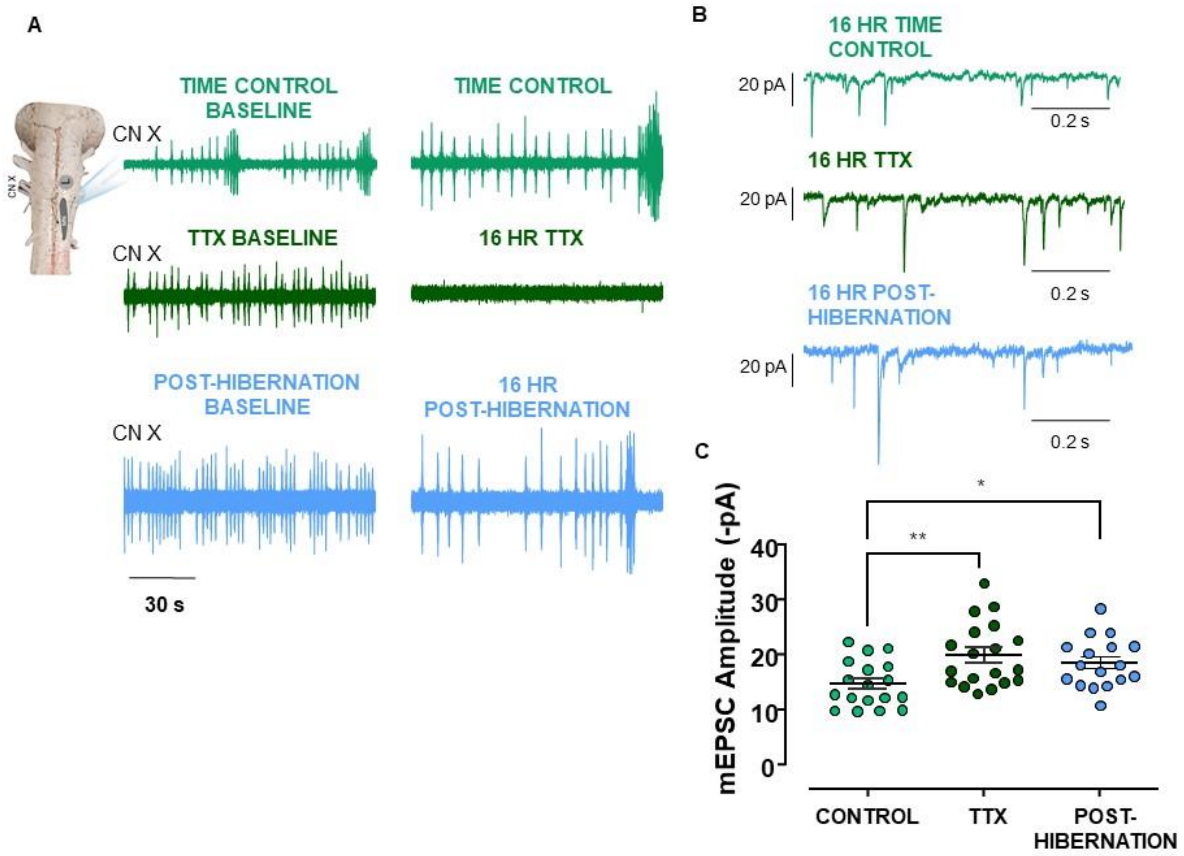

Figure 2 Hibernation and TTX both induce increases in mEPSC amplitude to the same extent. (A) Example respiratory-related motor output from the cut vagus nerve root (CN X) highlight activity for the entire incubation period. TTX silenced activity in all preparations (B) Example mEPSC traces recorded in whole-cell voltage clamp in laryngeal motoneurons in time control, TTX, and following hibernation. (C) Mean data showing enhanced mEPSC amplitude following both hibernation and TTX exposure relative to time control (One-way ANOVA, Holm-Sidak Multiple Comparisons Test, control vs. TTX, p=0.004, control vs. post-hibernation, p=0.0139, TTX vs. post-hibernation, p=0.4405). Circles represent cell-averaged mEPSCs for each neuron. Error bars are S.E.M. Horizontal line represents the mean. Control (n=18 from 5 animals), TTX (n=19 from 5 animals), post-hibernation (n=17 from 4 animals). *p<0.05, **p<0.01.

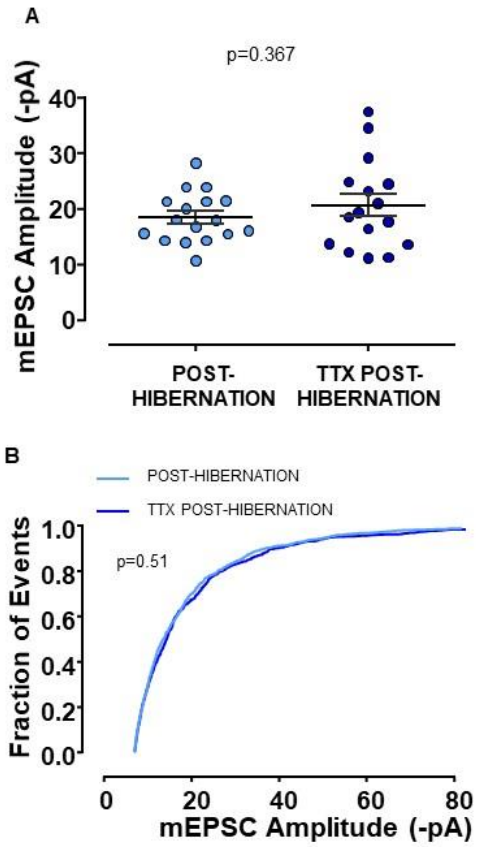

Figure 3 Hibernation occludes the mEPSC amplitude increase by TTX. (A) shows the mean mEPSC amplitude after hibernation and hibernation in the presence of 16 hr TTX (unpaired t test) and (B) shows the cumulative distribution (Kolmogorov-Smirnov Test). Circles represent cell-averaged mEPSCs for each neuron. Error bars are S.E.M. Horizontal line represents the mean.

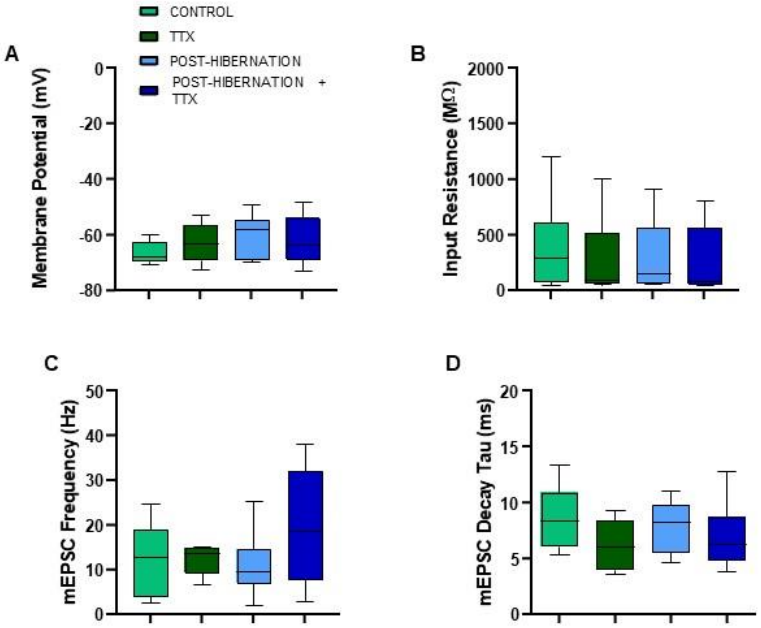

Figure 4 Membrane and other mEPSC properties are not affected following hibernation with or without activity in the post-hibernation period. (A-E) All variables were compared using a one-way ANOVA. No statistical difference was detected among treatments. Control (n=18), TTX (n=19), post-hibernation (n=17), post-hibernation+TTX (n=16). Box and whisker plots show the interquartile range. Whiskers extend to maximum and minimum values.

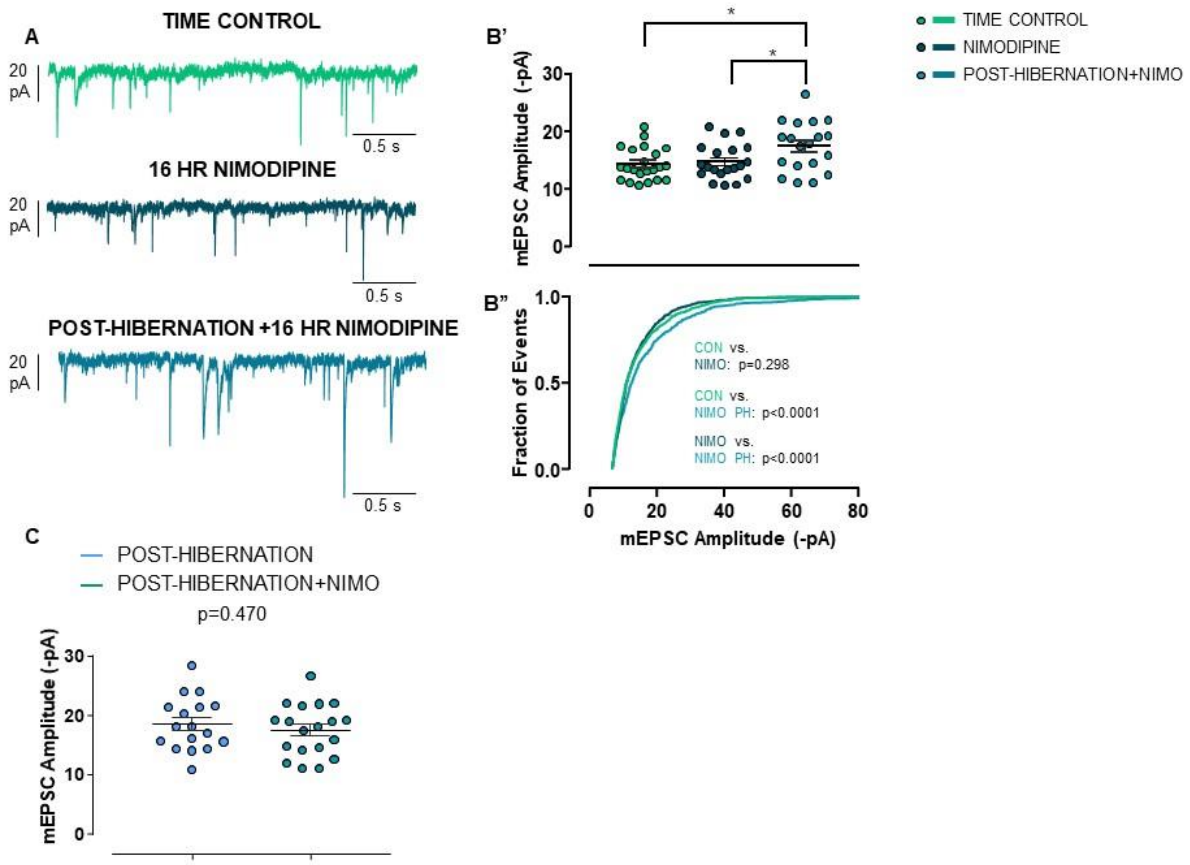

Figure 5 Block of L-type Ca^{2+} channels does not increase mEPSC amplitude. (A) Example mEPSC traces recorded in whole-cell voltage clamp in time control (n=22 from 6 animals), 10 µM nimodipine (n=20 from 5 animals), and post-hibernation+nimodipine (n=19 from 5 animals). (B') Cell-averaged mEPSC amplitudes and (B'') cumulative distribution of mEPSC amplitudes. Nimodipine exposure does not increase mean synaptic strength or alter the distribution of mEPSC amplitudes. After hibernation, exposure to nimodipine still results in enhanced synaptic strength (time control vs post-hibernation+nimodpine, p=0.0163; nimodipine vs. post-hibernation+nimodipine, p=0.0367). (C) Post-hibernation (n=17 from 5 animals) and post-hibernation+ nimodipine (n=19) have similar group means (unpaired t test). Circles represent cell-averaged mEPSCs for each neuron. Error bars are S.E.M. Horizontal line represents the mean. * indicates $p< 0.05$

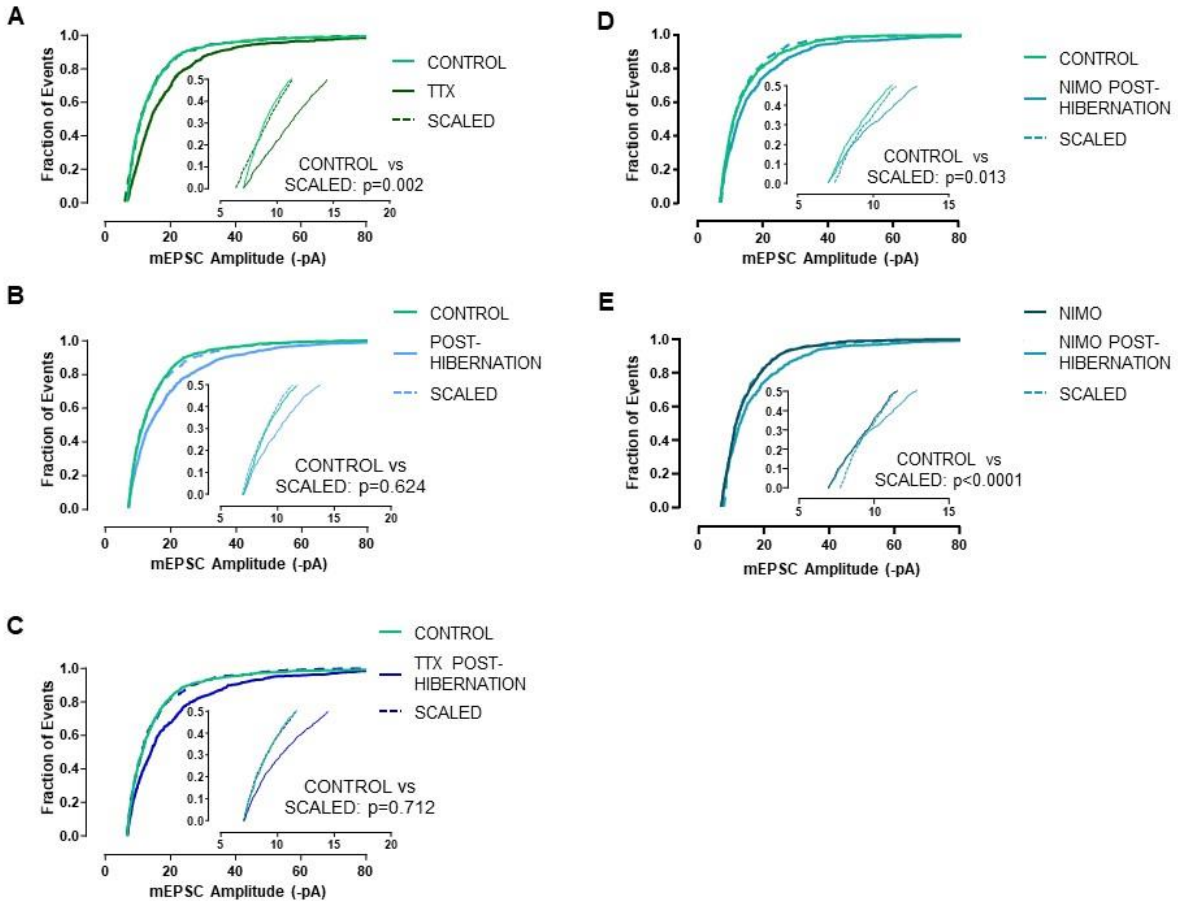

Figure 6 Hibernation, but not TTX, scales synapses, and multiplicative scaling is maintained by Ca^{2+} feedback . Cumulative distributions of mEPSC amplitudes for time control, treatment (TTX, post-hibernation, post-hibernation+TTX, post-hibernation+nimodipine), and mathematically downscaled treatment distributions. TTX does not lead to precise scaling of mEPSC amplitudes (A). Upregulated TTX mEPSCs were downscaled by the linear equation y=1.47x-2.21 (B) Hibernation and hibernation+TTX increases mEPSCs through multiplicative scaling (C). Upregulated hibernation mEPSCs were downscaled by the linear equation y=1.53x-3.58 and upregulated mEPSC after hibernation+TTX were downscaled by the equation y=1.61x-4.14. (D-E) After hibernation in the presence of nimodipine, mEPSC amplitudes were no longer increased according to multiplicative scaling. (D) uses time control as the control group and (E) uses the warm-acclimated nimodipine as the control. When using the time control as control, upregulated mEPSC amplitudes after hibernation+nimodipine were downscaled according to the equation, y=1.45x-3.76. When using nimodipine from warm acclimated animals as the control, upregulated mEPSCs were downscaled according to the equation y=1.52-4.75. All comparisons between control and treatment yielded p values <0.0001 (Kolmogorov-Smirnov Test.). P values shown in the figures compare control vs. scaled distributions (Kolmogorov-Smirnov Test).

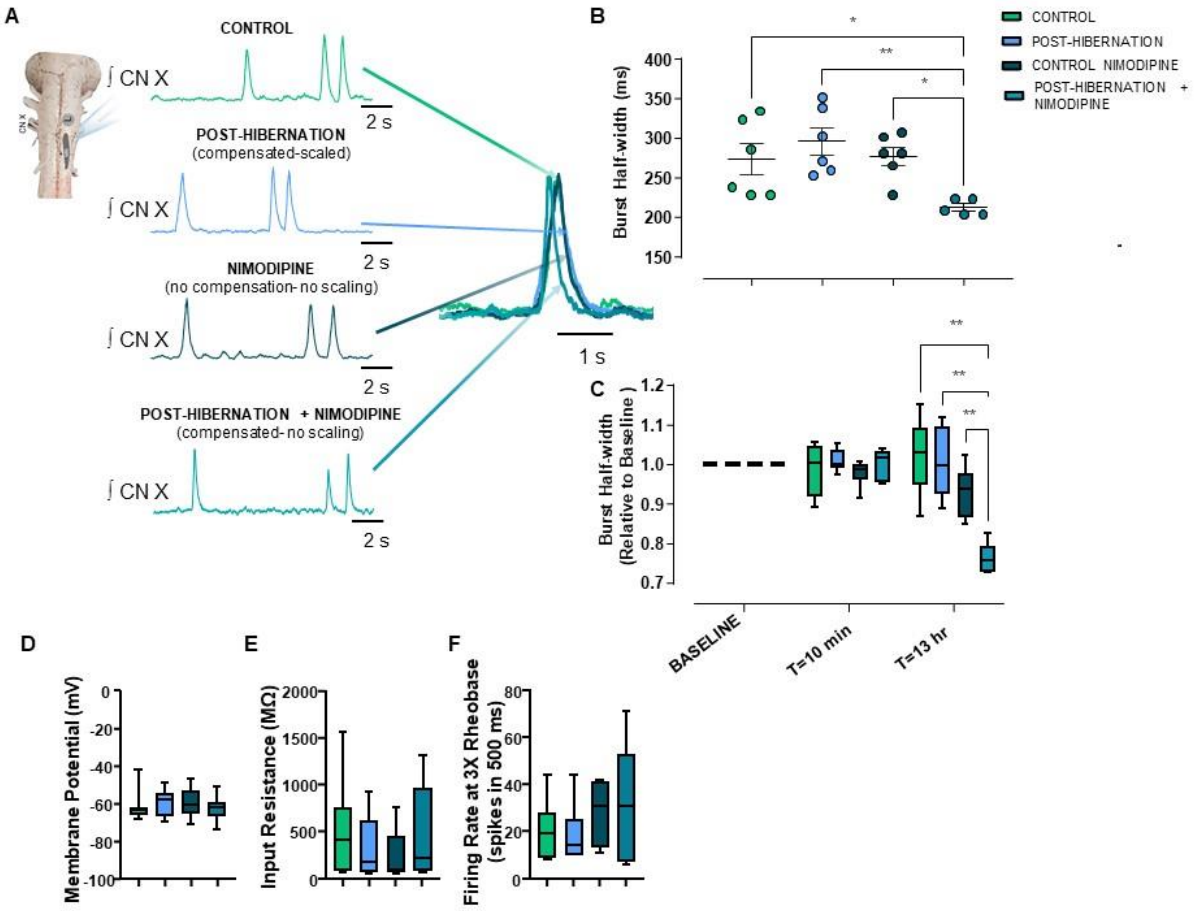

Figure 7 A failure to precisely scale motoneuron synaptic strength is associated with reduced respiratory motor outflow. (A) Simplified schematic of the brainstem preparation, highlighting integrated respiratory-related motor output recorded from the vagus nerve. The four groups shown are time control, post-hibernation (associated with scaled compensation), nimodipine in warm-acclimated control (no compensation, no scaling), and post-hibernation+nimodipine (unscaled compensation) for 13 hrs *in vitro*. Traces are compressed or expanded and overlayed to highlight differences across groups. (B) Nimodipine applied following hibernation resulted in narrower respiratory bursts from the vagus nerve (One-way ANOVA with Holm-Sidak's Multiple Comparisons Test; control vs. post-hibernation nimo, p=0.049, post-hibernation vs. posthibernation nimo, p=0.007, nimo vs posthibernation nimo=0.041). (C) Nimodipine resulted in a slow, reduction of burst width in the post-hibernation group, as acute exposure to nimodipine did not affect burst amplitude in any group (Two-way ANOVA followed by Holm-Sidak's multiple comparisons test). However, burst width decreases with longer exposure of nimodipine only after hibernation (p<0.01 relative to all other groups). n= 6,6,6, and 5 brainstem preparations for control, post-hibernation, nimodipine, and post-hibernation nimodipine, respectively. Intrinsic properties were not different across groups. Membrane potential (C), input resistance (D), firing frequency (at 3X rheobase; E). For (A), n= 6,6,6, and 5 brainstem preparations for control, post-hibernation, nimodipine,

and post-hibernation nimodipine, respectively. For (C &D), n= 20, 17, 20, and 19 neurons for control, post-hibernation, nimodipine, and post-hibernation+nimodpine, respectively. For assessment of firing rate (E), n= 7,6,6,7 neurons were used in control, post-hibernation, nimodipine, and post-hibernation+nimodpine, respectively. Box and whisker plots show the interquartile range. Whiskers extend to maximum and minimum values *$p<0.05$, **$p<0.01$.